Isotope Effect of Underdoped Cuprates in the Yang-Rice-Zhang Model

E. Schachinger · **J. P. Carbotte**

Abstract The underdoped region of the cuprates phase diagram displays many novel electronic phenomena both in the normal and the superconducting state. Many of these anomalous properties have found a natural explanation within the resonating valence bond spin liquid phenomenological model of Yang-Rice-Zhang (YRZ) which includes the rise of a pseudogap. This leads to Fermi surface reconstruction and profoundly changes the electronic structure. Here we extend previous work to consider the shift in critical temperature on ^{16}O to ^{18}O substitution, The isotope effect has been found experimentally to be very small at optimal doping yet to rapidly increase to very large values with underdoping. The YRZ model provides a natural explanation of this behavior and supports the idea of a pairing mechanism which is mainly spin fluctuations with a subdominant ($\sim 10\%$) phonon contribution.

1 Introduction

The isotope effect (α) which gives the change in critical temperature with ion mass played a significant role in the development of the BCS theory of conventional metals. It was widely interpreted to indicate that the electron-phonon interaction was involved in the mechanism of Cooper pair condensation. On the other hand, in the high T_c oxides at optimum doping α is an order of magnitude smaller [1,2] than the canonical BCS value of $1/2$ and this was taken as an early indication that the mechanism for superconductivity is different in the cuprates and is mainly electronic in nature. However, it was found that in the underdoped region of

E. Schachinger
Institute of Theoretical and Computational Physics
Graz University of Technology, NAWI Graz, A-8010 Graz, Austria
E-mail: schachinger@itp.tu-graz.ac.at

J. P. Carbotte
Department of Physics and Astronomy, McMaster University,
Hamilton Ont., Canada L8S 4M1
The Canadian Institute for Advanced Research, Toronto Ont., Canada M5G 1Z8

the phase diagram the isotope coefficient α increases rapidly and becomes larger than $1/2$ [1,2]. Dahm [3] provided a brief review of some of many possible explanations including the idea that important energy dependence in the electronic density of states (EDoS) at the Fermi level [4] on the scale of the superconducting energy can affect the isotope effect. Zeyher and Greco [5] used in comparison to Dahm a far more involved approach but also arrived at the conclusion that only a small contribution of electron-phonon interaction to the over all pairing potential is sufficient to explain the isotope effect in the underdoped cuprates.

Prominent kink like structures in the electronic dispersion curves of the cuprates measured in angular resolved photo-emission spectroscopy (ARPES) [6,7] have been widely interpreted as indication of the coupling of the charge carriers to boson modes. Some argued for phonons [6,7] while other authors favored coupling to a spin fluctuation resonant mode [8]. Additional information on the origin of the nodal direction dispersion kinks at $\sim 70\,$meV was provided by Iwasawa et $al.$ [9] who measured their change in optimally doped $Bi_2Sr_2CaCu_2O_{8+\delta}$ on oxygen substitution ^{16}O to ^{18}O. A recent scanning tunneling spectroscopy (STM) study [10] has also found a shift in a mode at $52\,$meV which is compatible with the expected amount on ^{16}O to ^{18}O substitution. A detailed analysis of the data on oxygen substitution was undertaken by Schachinger et $al.$ [11,12]. Within an Eliashberg formulation of a boson exchange mechanism one can invert ARPES [13] or infrared optical data (IR) [14,15] to recover the entire electron boson spectral density $I^2\chi(\omega)$ involved. This is a composite of phonon structures as well as spin fluctuation exchange processes or other excitations that could be coupled to the charge carriers and manifest in the electron boson spectral density $I^2\chi(\omega)$ [16]. Using such an information Schachinger et $al.$ [11] concluded that the substitution data of Iwasawa et $al.$ [9] can be understood as arising from a phonon peak in $I^2\chi(\omega)$ which accounted for about 10% of the total spectral weight associated with the electron boson spectral density. Furthermore, Dal Conte et $al.$ [17] reported a phonon contribution of approx. 20% to the electron boson spectral density in the system $Bi_2Sr_2Ca_{0.92}Y_{0.08}Cu_2O_{8+\delta}$ using a very different type of analysis. All this puts a serious constraint on the resulting isotope effect and is compatible with the very small value of $\alpha \simeq 0.05$ found in the optimally doped cuprates. The question then arises of how this observation is compatible with the very large increase in α found as doping is reduced. One should keep in mind that the properties of the superconducting state are also observed to evolve away from a BCS description with d-wave superconducting gap symmetry even though such a model provides a good qualitative description of the optimum and overdoped region of the cuprate phase diagram. The observed deviations go beyond what can be understood when anisotropy [18,19,20,21,22,23], energy dependence in the EDoS [24,25] or when inelastic and strong coupling corrections [26,27,28] are introduced in a generalized Eliashberg description. Many of these anomalous properties can, however, be understood within the semi phenomenological model of Yang, Rice, and Zhang (YRZ) [29,30,31] of the pseudogap state of the underlying normal state [32,33] of the underdoped cuprates which do not behave like Fermi liquids would. This model is based on ideas of the resonant valence bond (RVB) [34] spin liquid and provides a specific ansatz for the normal state self energy. When generalized to include superconductivity it has been remarkably successful in providing a first understanding of the, until then, anomalous properties [32,33] associated with the formation of a pseudogap. This is accompanied with Fermi surface (FS) reconstruction from the large FS of Fermi liquid theory to closed Luttinger pockets centered about the nodal direction in the copper-oxygen plane Brillouin zone (BZ). As half filling is approached the pockets become progressively smaller. In this model metallicity is lost not through an ever increasing effective mass. Rather the quasiparticles remain light in the nodal direction

while the antinodal regions [35] are completely gaped out. As a consequence, the in-plane resistivity remains metallic [36] as observed [37,38]. For example, Lee *et al.* [39] found that a Drude response remains well inside the antiferromagnetic dome seen at small doping beyond the end of the superconducting dome. At the same time the model can explain an insulating c-axis dc-response [37,38] within a coherent c-axis charge transfer model which eliminates c-axis transport because the plane to plane matrix element has d-wave symmetry and is zero in the nodal directions [40,41]. Among the many results obtained in the literature we mention here a representative set which shows that the YRZ model is capable of providing a first understanding of most of the anomalous superconducting properties seen in the underdoped cuprates. A review can be found in the paper by Rice *et al.* [42] which also provides elaboration of the theoretical basis of the YRZ ansatz.

Yang *et al.* [31,43] showed that the particle-hole asymmetry observed in ARPES as one moves off the nodal direction in the pseudogap state can be understood both in terms of their energy value and their quasi particle spectral weight. LeBlanc *et al.* [44] also discussed the effect of a particle-hole asymmetric pseudogap on the Bogliubov quasiparticles and found reasonable agreement with ARPES data of Hashimoto *et al.* [45]. Yang *et al.* [46] showed that there exists fully enclosed hole Luttinger pockets and that the spectral weight of the FS on the antiferromagnetic side of the BZ is small as compared with the spectral weight on the other face of the pocket oriented towards the Γ-point. Both shape and area enclosed in the pockets are in agreement with the YRZ model. STM can also be used to get detailed FS data as found in the work of Kohsaka *et al.* [47] for example. The observed interference patterns due to impurity scattering are analyzed to yield FS contours and, possibly, details of the pseudogap Dirac point [48]. Bascones and Valenzuela [49] addressed the issue of checkerboard patterns observed in STM. The total EDoS can also be obtained from STM data. Borne *et al.* [50] provided an analysis of the STM data of Pushp *et al.* [51] and found good agreement with YRZ, confirming an earlier result of Yang *et al.* [31] who compared with STM data of Kohsaka *et al.* [47]. The low temperature (T) specific heat [52,53,54] was found to remain linear in T deep inside the underdoped regime. This observation provides clear evidence that the quasiparticles around the nodes which is the only region sampled at low T remain BCS like. At the same time the specific heat is strongly suppressed below its BCS value as T is increased towards T_c because now the pseudogap region of the BZ zone is sampled. A similar situation holds for the in-plane penetration depth which remains linear in T at low T but becomes suppressed over its optimal value as T is increased towards T_c. In fact both, experiment [55] and theory [56] find a quasilinear in T dependence over the entire interval from $T = 0$ to $T = T_c$. The behavior of the c-axis penetration depth can also be understood in YRZ [57]. Other studies involve the in-plane ac optical conductivity [58, 59,60], the optical scattering rates [61] as well as the c-axis optical response [62,63,64] for both coherent and incoherent charge transfer in the direction perpendicular to the copper-oxide planes. The c-axis sum rule, long not understood, also follows in YRZ theory [65]. In a Fermi liquid the optical spectral weight under the real part of the optical conductivity is unchanged when the superconducting state is entered. For the underdoped cuprates measurements [66] of the c-axis optical weight found a serious violation of this sum rule. The Raman response [49,67,68,69,70] of the underdoped cuprates is particularly interesting. The peak position in the B2g response which preferentially samples the nodal response, is found to decrease with decreasing doping while the B1g response which samples mainly the antinodal region of the BZ shows the opposite trend, i.e. increases in energy. This is in agreement with a superconducting gap which decreases while the pseudogap increases, a well documented phenomenon [71] in the cuprate phase diagram. A comparison of YRZ predictions and experimental data of the Andreev and single particle tunneling spectra by Yang *et al.*

[72] provides further support for the two gap model with distinct superconducting and RVB gap. The pseudogap also modifies the universal limits [73,74] of the optical and thermal conductivity [75,76]. Impurity scattering, again, drops out in this limit but Gutzwiller factors associated with the effects of strong correlations appear. These are not part of a Fermi liquid description. A detailed comparison of the dynamical spin susceptibility calculated in YRZ by James *et al.* [77] with both inelastic neutron and resonant X-ray scattering data found satisfactory qualitative agreement at all energy scales considered including the known hourglass pattern for the magnetic susceptibility.

All of the above described properties have aspects that cannot be understood within a conventional d-wave BCS framework but find a natural explanation when the YRZ model is used to describe the underlying normal state with the underlying emergence of a pseudogap. With this success highlighted, it is important to know whether or not the observed large increase in isotope effect with decreased doping towards the Mott insulating state can also be explained to be a result of pseudogap formation. A very simple model of pseudogap formation on the isotope coefficient α has already appeared [3] and it has been found that α increases steadily as the magnitude of the pseudogap is cranked up without changing the amount of the pairing potential that is taken to be due to phonons as compared to the dominating part coming from an electronic mechanism. This provided further motivation to apply to this problem the more realistic YRZ model which includes FS reconstruction into Luttinger pockets. The parameters of the band structure and pseudogap used in the original YRZ paper will not be altered as it lead to good agreement with a large data set. The observation that only about 10% of the pairing interaction in the electron boson spectral density can come from phonons will be respected and represents a constraint on the work.

In Sec. 2 we summarize the results associated with FS reconstruction brought about by the emergence of a finite pseudogap below a quantum critical point (QCP) at doping $x = x_c$. The superconducting state with gap of d-wave symmetry is considered in Sec. 3 where we also present results for the isotope effect. Finally, Sec. 4 contains a discussion and our conclusions.

2 Formalism Normal State

In the YRZ model the coherent part of the charge carrier Green's function for doping x has the form [31]

$$G^N(\mathbf{k}, \omega; x) = \sum_{\alpha=\pm} \frac{g_t(x) W_{\mathbf{k}}^{\alpha}(x)}{\omega - E_{\mathbf{k}}^{\alpha}(x)}, \tag{1}$$

where $g_t(x) = 2x/(1+x)$ is a Gutzwiller factor that enters the theory of strongly correlated electrons and relates to the exclusion of double occupancy because of the strong on-site Hubbard U. If the pseudogap $\Delta_{pg}(\mathbf{k}, x)$ is finite there are two branches $(+/-)$ to the normal state energies, namely

$$E_{\mathbf{k}}^{\pm}(x) = \frac{\varepsilon_{\mathbf{k}}(x) - \varepsilon_{\mathbf{k}}^{\circ}(x)}{2} \pm \sqrt{\Delta_{pg}^2(\mathbf{k}, x) + \{[\varepsilon_{\mathbf{k}}(x) + \varepsilon_{\mathbf{k}}^{\circ}(x)]/2\}^2} \tag{2}$$

and these are further weighted by factors

$$W_{\mathbf{k}}^{\pm}(x) = \frac{1}{2} \left\{ 1 \pm \frac{\varepsilon_{\mathbf{k}}(x) + \varepsilon_{\mathbf{k}}^{\circ}(x)}{2\sqrt{\left[\frac{\varepsilon_{\mathbf{k}}(x) + \varepsilon_{\mathbf{k}}^{\circ}(x)}{2}\right]^2 + \Delta_{pg}^2(\mathbf{k}, x)}} \right\}. \tag{3}$$

The electron dispersion curves $\varepsilon_{\mathbf{k}}(x)$ as a function of momentum $\mathbf{k}$ describe the electronic structure when no account is taken of the pseudogap. It involves up to third nearest neighbor hoping as well as the magnetic energy scale J of the $t-J$ model and an additional Gutzwiller factor $g_s(x) = 1/(1+x)^2$. Details of these dispersion curves are found in the original paper of YRZ [29] and will not be altered here. The energy $\varepsilon_{\mathbf{k}}^{\circ}(x)$ involves only first nearest neighbor hopping t_0 and $\varepsilon_{\mathbf{k}}^{\circ}(x) = 0$ gives the boundary of the antiferromagnetic Brilloin zone (AFBZ). The AFBZ corresponds to half filling $(x=0)$ which would be metallic if the pseudogap was not accounted for but in reality is the Mott insulating state. It is important to note that in the limit $\Delta_{pg}(\mathbf{k},x) \to 0$ the Green's function $G^N(\mathbf{k},\omega;x)$ reduces to its usual form, namely $(\omega - \varepsilon_{\mathbf{k}})^{-1}$. The pseudogap $\Delta_{pg}(\mathbf{k},x)$ is taken to have d-wave symmetry in the BZ with its amplitude linear in x, increasing with decreasing doping and zero at optimum doping where the critical temperature for superconductivity has its maximum. At optimum doping taken to be $x_c = 0.2$ in YRZ there is no pseudogap and the FS is the large contour of Fermi liquid theory shown as the dash-dotted (blue) line in Fig. 1(a) where the top right quadrant of the CuO_2 BZ is shown as a function of k_x/a and k_y/a with a the lattice parameter. The short dotted (black) line on the diagonal is the AFBZ. Also shown is the reconstructed FS [solid and dashed (red) line] when $x = 0.12$ and there is a finite pseudogap. The enclosed area is the Luttinger hole pocket which we have shaded (green) for emphasis. The back side of the Luttinger pocket [dashed (red) line] has small weighting as compared to the side pointing towards [solid (red) line] the Γ-point in the BZ leading approximately to the concept of a Fermi arc [78]. As the doping is further reduced towards the Mott insulating state, the Luttinger pocket shrinks even more. Nevertheless, a small number of quasiparticles remains along the nodal direction $\overline{\Gamma M}$. It is in this way that the metallicity is reduced and eventually lost.

3 Formalism Superconducting State

We want to build up a superconducting state based on the normal state which describes the underdoped region of the cuprate phase diagram rather than on an underlying Fermi liquid band structure described by the dispersion curves $\varepsilon_{\mathbf{k}}(x)$. For a given pairing potential $V_{\mathbf{k},\mathbf{k}'}$ one can then proceed to write down the superconducting Green's function in the usual way

$$G^s(\mathbf{k},\omega,x) = \sum_{\alpha=\pm} \frac{g_t(x)W_{\mathbf{k}}^{\alpha}(x)}{\omega - E_{\mathbf{k},s}^{\alpha}(x) - \frac{\Delta_{sc}^2(\mathbf{k},x)}{\omega + E_{\mathbf{k},s}^{\alpha}(x)}}, \tag{4}$$

where the new energies $E_{\mathbf{k},s}^{\pm} \equiv \sqrt{[E_{\mathbf{k}}^{\pm}(x)]^2 + \Delta_{sc}^2(\mathbf{k},x)}$. The gap equation at temperature T takes the form [79]:

$$\Delta_{sc}(\mathbf{k},T,x) = -\sum_{\mathbf{k}',\alpha=\pm} V_{\mathbf{k},\mathbf{k}'} W_{\mathbf{k}'}^{\alpha}(x) \frac{\Delta_{sc}(\mathbf{k}',T,x)}{2E_{\mathbf{k}',s}^{\alpha}(T,x)} \tanh\left(\frac{E_{\mathbf{k}',s}^{\alpha}(T,x)}{2T}\right). \tag{5}$$

Here we included for the first time explicitly the temperature T in the gap. As we are here interested only in the critical temperature T_c Eq. (5) can be linearized in $\Delta_{sc}(\mathbf{k},T,x)$ to give:

$$\Delta_{sc}(\mathbf{k},T,x) = -\sum_{\mathbf{k}',\alpha=\pm} V_{\mathbf{k},\mathbf{k}'} W_{\mathbf{k}'}^{\alpha}(x) \frac{\Delta_{sc}(\mathbf{k}',T,x)}{2|E_{\mathbf{k}'}^{\alpha}(T,x)|} \tanh\left(\frac{E_{\mathbf{k}'}^{\alpha}(T,x)}{2T_c}\right). \tag{6}$$

This equation has the usual form of the normal BCS T_c equation except that now the pseudogap is built into the energies $E_{\mathbf{k}'}^{\alpha}(x)$ and these go to zero only on the Luttinger Fermi contours
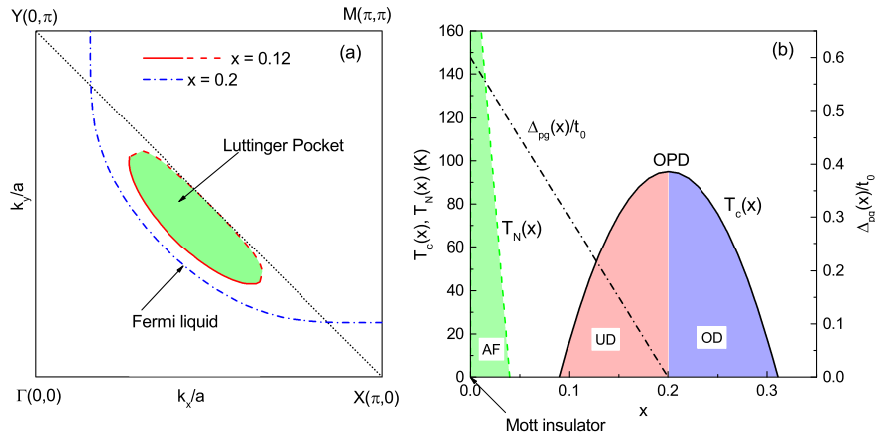
Fig. 1 (Color online)(a) The right hand upper quadrant of the Cu_2O BZ with momentum **k** in units of the lattice parameter a. The dashed dotted (blue) curve is the Fermi liquid large FS at optimum doping ($x = 0.2$) where there is no pseudogap. The short dotted (black) diagonal represents the AFBZ boundary. The solid and dashed (red) contour is the FS for the case $x = 0.12$ where the pseudogap has lead to its reconstruction into a small Luttinger pocket [shaded (green) area] centered about the diagonal $\overline{\Gamma M}$. (b) A schematic view of the cuprate phase diagram. The dashed dotted (black) line (right hand scale applies) shows the pseudogap amplitude normalized to t_0, $\Delta_{pg}(x)/t_0 = 3(0.2 - x)$, as a function of doping x in the YRZ model. The solid (black) dome gives the superconducting critical temperature $T_c(x)$ vs x (left hand scale applies) with optimal doping (OPD) indicated as the dome maximum with the overdoped (OD) [shaded (blue)] area on the right and the underdoped (UD) [shaded (red)] area on the left. We also indicated the antiferromagnetic (AF) region [shaded (green) area] with the Néel temperature $T_N(x)$ and the Mott insulating state at $x = 0$.

which define the Luttinger pockets of Fig. 1(a). To proceed we need a model for the pairing potential. Two possible models were studied in Ref. [79] with very similar results. Here it will be sufficient to take only one, namely

$$V_{\mathbf{k},\mathbf{k}'} = -g(x)U_{nn}\{\cos[(k_x - k_{x'})/a] + \cos[(k_y - k_{y'})/a]\}, \qquad (7)$$

where the nearest neighbor interaction U_{nn} is set equal to $75\,\text{meV}$ which leaves one single parameter $g(x)$. The superconducting dome shown in the cuprate phase diagram Fig. 1(b) [solid (black) line] is an empirical quantity given by

$$T_c(x) = 95.0[1 - 82.6(x - 0.2)^2], \qquad (8)$$

where $T_c(x)$ is given in Kelvin. Optimum doping ($x = 0.2$) gives a maximum T_c of $95\,\text{K}$ which is characteristic of YBCO. To the right is the overdoped [shaded (blue)] and to the left the underdoped region [shaded (red)]. Near $x = 0$ is an antiferromagnetic region [shaded (green)] as the Mott insulating state is approached. Equation (7) is used to determine the value of $g(x)$ for any doping below $x = 0.2$ which covers the underdoped region with finite pseudogap and reconstructed FS into Luttinger hole pockets. The results obtained are summarized in Fig. 2 where we plot T_c as a function of doping x [solid (black) curve, left hand
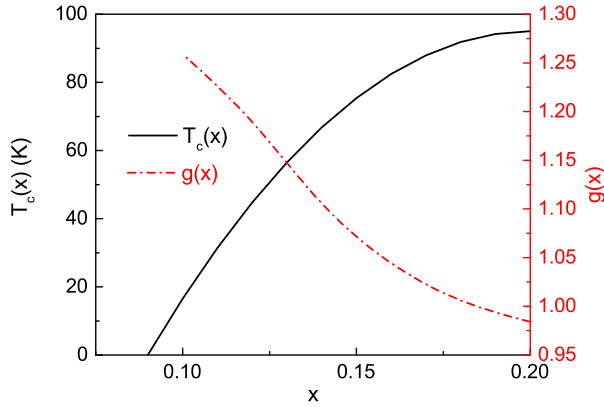
Fig. 2 (Color online) The coupling constant $g(x)$ [dashed dotted (red) line, right hand scale] as a function of doping x which is needed in the nearest neighbor pairing model [Eq. (7)] to reproduce the measured value of T_c as a function of x [solid (black) curve, left hand scale] in the underdoped region of the cuprate phase diagram Fig. 1(b).

scale] and the resulting value of $g(x)$ [dashed dotted (red) curve, right hand scale]. We see that to reproduce the measured value of T_c, $g(x)$ needs to increase as doping is reduced towards the Mott insulating state. This may be an indication that the spin fluctuations increase as the antiferromagnetic region of the phase diagram, which falls somewhat below the end of the superconducting dome, is approached.

To discuss the isotope effect at any doping x we break up $g(x)$ into two contributions. A sub-dominant phonon contribution which accounts for 5 to 10% of the total value of $g(x)$ and a second, dominant piece, electronic in origin, which accounts for the rest 95 to 90%. A phonon cut-off at $\omega_D = 80\,$meV is also applied to the phonon contribution and the over all magnitude of the coupling g is changed to get the measured value of T_c. The phonon cut-off is further shifted according to the square root of the ratio of the oxygen 16 to 18 mass (M) and the calculation of T_c is repeated, the change in T_c noted and α is then determined from $T_c \propto M^{-\alpha}$. Results for $\alpha(x)$ vs x are presented in Fig. 3 where we plot the ratio α to its value at optimum doping α_{op} as a function of the normalized temperature $T_c(x)/T_c^{op}$. Both the case of a 5% and 10% phonon contribution to the total pairing are presented as the solid (black) and dashed (red) curves, respectively. We see that α which is small at optimum doping rapidly increases as x is decreased into the underdoped region of the phase diagram. This demonstrates that the existence of a pseudogap can drastically increase the isotope effect over its Fermi liquid value obtained when $\Delta_{pg}(x)$ is set equal to zero. We also show in Fig. 3 experimental results of Franck *et al.* [1,2] obtained for Pr doped YBCO as solid squares. It is clear that the YRZ model of the underdoped cuprates can naturally provide an explanation for the anomalous isotope effect observed in the underdoped cuprates and requires only a 5% to 10% contribution to the pairing potential to originate in the electron-phonon interaction. This is in line with a large body of other information on the electron-boson spectral density in the cuprates which indicate that the major contribution to the pairing glue comes from the exchange of excitations of electronic origin, probably spin fluctuations [16]. Our results are generic and do not depend sensitively on details. Rather they have their base in the growth of the pseudogap which provides an energy dependence to the EDoS. Because we
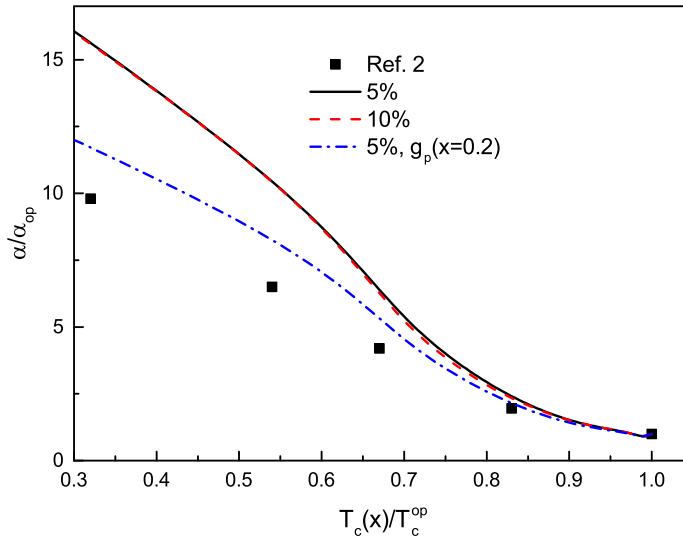
Fig. 3 (Color online) The isotope effect α normalized to its value α_{op} at optimum doping as a function of the ratio of the critical temperature $T_c(x)$ to its value at optimum doping T_c^{op} ($x = 0.2$ in our model). The solid (black) curve is for a 5% contribution of phonons to the total pairing coupling constant $g(x)$ of Eq. (7) while the dashed (red) curve is for a 10% contribution. The dashed-dotted (blue) curve leaves the phonon contribution at its value at optimum doping. The solid black squares are the data of Ref. [2] for Pr doped YBCO.

used a BCS type approach we cannot expect quantitative agreement with experiment but the qualitative agreement obtained is robust and the large increase in α observed is easily understood with a rather modest magnitude of electron-phonon coupling. The dashed-dotted (blue) curve serves to emphasis the point that the exact strength of the electron-phonon interaction assumed does not change the general trend seen in Fig. 3. To arrive at this curve the electron-phonon part of the pairing was kept at its value obtained at optimum doping, i.e. $x = 0.2$. This assumption gives better agreement with experiment than when $g_p(x)$ is increased slightly with decreasing values of x in direct proportion to the over all $g(x)$ which, as we saw in Fig. 2 [dashed-dotted (red) curve] must increase with decreasing x so that $T_c(x)$ stays on the measured superconducting dome [solid (black) curve].

4 Summary and Conclusion

The normal state electronic properties of the underdoped cuprates cannot be understood within a Fermi liquid framework. Moreover, the observed superconducting state properties also do not conform, even qualitatively, to the behavior expected in a BCS model extended to include the d-wave symmetry of the superconducting gap function. An additional element is required which goes beyond extensions such as anisotropy, energy dependent EDoS, inelastic scattering, or other elaborations which have played some role in the superconductivity of conventional metals. Strong correlations effects become essential as the Mott insulating

state is approached with reduced doping and a pseudogap is seen to emerge in the normal state. How this feature is to be described, however, remains controversial. A prominent model which has recently shown great promise is the resonating valence bond spin liquid model developed by Yang *et al.* [29]. These authors provided a simple phenomenological ansatz for the self energy in the pseudogap state which has proved very successful in understanding anomalous normal as well as superconducting state properties. We provided in this paper a brief review of these successes to set the context for the present work. The model involves a quantum critical point at doping $x = x_c$ below which the pseudogap rises in magnitude and strongly modifies the electronic structure including the reconstruction of the FS from the large contour of Fermi liquid theory to small Luttinger hole pockets centered about the nodal direction in the copper-oxygen BZ and near the AFBZ. The energy scale associated with the pseudogap is comparable to the superconducting gap scale and this alters profoundly superconducting properties as has been documented here by providing a brief survey of recent literature. A conclusion of such work is that, in a large part, YRZ can provide a natural and straight forward understanding of a large variety of properties previously considered anomalous. Here we extended the work to the isotope effect with equal success. At optimum doping the observed change in critical temperature with $^{16}O \rightarrow {}^{18}O$ substitution is found to be very small and much less than the BCS prediction for an electron-phonon system. This observation is consistent with the great deal of independent knowledge pointing to the fact that the driving mechanism for superconductivity in the cuprates is mainly electronic in nature. The evidence [16] also points to a subdominant contribution from phonons which is consistent with a small, nonzero isotope effect. As the doping is reduced below optimum doping the pseudogap provides a new energy dependence to the EDoS and, as we find here, this can increase radically the isotope effect. This increase is generic to such models and requires only a minor contribution to the total pairing potential to originate from the electron-phonon interaction. Our calculations are quite consistent with experimental findings and add another property of the underdoped cuprates that finds a natural understanding within the YRZ model.

References

1. J.P. Franck, J. Jung, M.A.K. Mohamed, S. Gygax, G.I. Sproule, Phys. Rev. B **44**, 5318 (1991). DOI 10.1103/PhysRevB.44.5318
2. J.P. Franck, in *Physical Properties of High Temperature Superconductors*, vol. IV, ed. by D.M. Ginsberg (World Scientific, Singapore, 1994), vol. IV, p. 189
3. T. Dahm, Phys. Rev. B **61**, 6381 (2000). DOI 10.1103/PhysRevB.61.6381
4. E. Schachinger, M.G. Greeson, J.P. Carbotte, Phys. Rev. B **42**, 406 (1990). DOI 10.1103/PhysRevB.42.406
5. R. Zeyher, A. Greco, Phys. Rev. B **80**, 064519 (2009). DOI 10.1103/PhysRevB.80.064519
6. P.V. Bogdanov, A. Lanzara, S.A. Kellar, X.J. Zhou, E.D. Lu, W.J. Zheng, G. Gu, J.I. Shimoyama, K. Kishio, H. Ikeda, R. Yoshizaki, Z. Hussain, Z.X. Shen, Phys. Rev. Lett. **85**, 2581 (2000). DOI 10.1103/PhysRevLett.85.2581
7. A. Lanzara, P.V. Bogdanov, X.J. Zhou, S.A. Kellar, D.L. Feng, E.D. Lu, T. Yoshida, H. Eisaki, A. Fujimori, K. Kishio, J.I. Shimoyama, T. Noda, S. Uchida, Z. Hussain, Z.X. Shen, Nature (London) **412**, 510 (2001). DOI 10.1038/35087518
8. P.D. Johnson, T. Valla, A.V. Fedorov, Z. Yusof, B.O. Wells, Q. Li, A.R. Moodenbaugh, G.D. Gu, N. Koshizuka, C. Kendziora, S. Jian, D.G. Hinks, Phys. Rev. Lett. **87**, 177007 (2001). DOI 10.1103/PhysRevLett.87.177007

9. H. Iwasawa, J.F. Douglas, K. Sato, T. Masui, Y. Yoshida, Z. Sun, H. Eisaki, H. Bando, A. Ino, M. Arita, K. Shimada, H. Namatame, M. Taniguchi, S. Tajima, S. Uchida, T. Saitoh, D.S. Dessau, Y. Aiura, Phys. Rev. Lett. **101**, 157005 (2008). DOI 10.1103/PhysRevLett.101.157005
10. J. Lee, K. Fujita, K. McElroy, J.A. Slezak, M. Wang, Y. Aiura, H. Bando, M. Ishikado, T. Masui, J.X. Zhu, A.V. Balatsky, H. Eisaki, S. Uchida, J.C. Davis, Nature (London) **442**, 546 (2006). DOI 10.1038/nature04973
11. E. Schachinger, J.P. Carbotte, T. Timusk, EPL (Europhysics Letters) **86**, 67003 (2009). DOI 10.1209/0295-5075/86/67003
12. E. Schachinger, J.P. Carbotte, Phys. Rev. B **81**, 014519 (2010). DOI 10.1103/PhysRevB.81.014519
13. E. Schachinger, J.P. Carbotte, Phys. Rev. B **80**, 094521 (2009). DOI 10.1103/PhysRevB.80.094521
14. J. Yang, D. Hüvonen, U. Nagel, T. Rõõm, N. Ni, P.C. Canfield, S.L. Bud'ko, J.P. Carbotte, T. Timusk, Phys. Rev. Lett. **102**, 187003 (2009). DOI 10.1103/PhysRevLett.102.187003
15. J. Yang, J. Hwang, E. Schachinger, J.P. Carbotte, R.P.S.M. Lobo, D. Colson, A. Forget, T. Timusk, Phys. Rev. Lett. **102**, 027003 (2009). DOI 10.1103/PhysRevLett.102.027003
16. J.P. Carbotte, T. Timusk, J. Hwang, Reports on Progress in Physics **74**, 066501 (2011). DOI 10.1088/0034-4885/74/6/066501
17. S. Dal Conte, C. Giannetti, G. Coslovich, F. Cilento, D. Bossini, T. Abebaw, F. Banfi, G. Ferrini, H. Eisaki, M. Greven, A. Damascelli, D. van der Marel, F. Parmigiani, Science **335**, 1600 (2012). DOI 10.1126/science.1216765
18. C.R. Leavens, J.P. Carbotte, Can. J. Phys. **49**(6), 724 (1971). DOI 10.1139/p71-088
19. H.K. Leung, J.P. Carbotte, D.W. Taylor, C.R. Leavens, Can. J. Phys. **54**(15), 1585 (1976). DOI 10.1139/p76-187
20. C. O'Donovan, J.P. Carbotte, Phys. Rev. B **52**, 4568 (1995). DOI 10.1103/PhysRevB.52.4568
21. C. O'Donovan, J.P. Carbotte, Phys. Rev. B **52**, 16208 (1995). DOI 10.1103/PhysRevB.52.16208
22. C. O'Donovan, J.P. Carbotte, Physica C **252**, 87 (1995). DOI 10.1016/0921-4534(95)00451-3
23. D. Branch, J.P. Carbotte, Phys. Rev. B **52**, 603 (1995). DOI 10.1103/PhysRevB.52.603
24. B. Mitrović, J.P. Carbotte, Can. J. Phys. **61**(5), 758 (1983). DOI 10.1139/p83-097
25. B. Mitrović, J.P. Carbotte, Can. J. Phys. **61**(5), 784 (1983). DOI 10.1139/p83-098
26. E.J. Nicol, J.P. Carbotte, Phys. Rev. B **44**, 7741 (1991). DOI 10.1103/PhysRevB.44.7741
27. J.P. Carbotte, C. Jiang, D.N. Basov, T. Timusk, Phys. Rev. B **51**, 11798 (1995). DOI 10.1103/PhysRevB.51.11798
28. J. Hwang, J. Yang, T. Timusk, S.G. Sharapov, J.P. Carbotte, D.A. Bonn, R. Liang, W.N. Hardy, Phys. Rev. B **73**, 014508 (2006). DOI 10.1103/PhysRevB.73.014508
29. K.Y. Yang, T.M. Rice, F.C. Zhang, Phys. Rev. B **73**, 174501 (2006). DOI 10.1103/PhysRevB.73.174501
30. R.M. Konik, T.M. Rice, A.M. Tsvelik, Phys. Rev. Lett. **96**, 086407 (2006). DOI 10.1103/PhysRevLett.96.086407
31. K.Y. Yang, H.B. Yang, P.D. Johnson, T.M. Rice, F.C. Zhang, EPL (Europhysics Letters) **86**(3), 37002 (2009). DOI 10.1209/0295-5075/86/37002
32. T. Timusk, B. Statt, Rep. Prog. Phys. **62**(1), 61 (1999). DOI 10.1088/0034-4885/62/1/002
33. M.R. Norman, D. Pines, C. Kallin, Adv. in Physics **54**, 715 (2005). DOI 10.1080/00018730500459906
34. P.W. Anderson, Science **235**, 1196 (1987). DOI 10.1126/science.235.4793.1196
35. J. LeBlanc, J. Carbotte, J. Supercon. and Novel Magnetism **24**, 2053 (2011). DOI 10.1007/s10948-011-1169-6
36. P.E.C. Ashby, J.P. Carbotte, Phys. Rev. B **87**, 014514 (2013). DOI 10.1103/PhysRevB.87.014514
37. T. Ito, K. Takenaka, S. Uchida, Phys. Rev. Lett. **70**, 3995 (1993). DOI 10.1103/PhysRevLett.70.3995
38. K. Takenaka, K. Mizuhashi, H. Takagi, S. Uchida, Phys. Rev. B **50**, 6534 (1994). DOI 10.1103/PhysRevB.50.6534
39. Y.S. Lee, K. Segawa, Z.Q. Li, W.J. Padilla, M. Dumm, S.V. Dordevic, C.C. Homes, Y. Ando, D.N. Basov, Phys. Rev. B **72**, 054529 (2005). DOI 10.1103/PhysRevB.72.054529
40. A. Levchenko, T. Micklitz, M.R. Norman, I. Paul, Phys. Rev. B **82**, 060502(R) (2010). DOI 10.1103/PhysRevB.82.060502
41. T. Xiang, J.M. Wheatley, Phys. Rev. Lett. **77**, 4632 (1996). DOI 10.1103/PhysRevLett.77.4632
42. T.M. Rice, K.Y. Yang, F.C. Zhang, Rep. Prog. Phys. **75**, 016502 (2012). DOI 10.1088/0034-4885/75/1/016502
43. H.B. Yang, J.D. Rameau, P.D. Johnson, T. Valla, A. Tsvelik, G.D. Gu, Nature (London) **456**, 77 (2008). DOI 10.1038/nature07400
44. J.P.F. LeBlanc, J.P. Carbotte, E.J. Nicol, Phys. Rev. B **83**, 184506 (2011). DOI 10.1103/PhysRevB.83.184506
45. M. Hashimoto, R.H. He, K. Tanaka, J.P. Testaud, W. Meevasana, R.G. Moore, D. Lu, H. Yao, Y. Yoshida, H. Eisaki, T.P. Devereaux, Z. Hussain, Z.X. Shen, Nature Phys. **6**, 414 (2010). DOI 10.1038/nphys1632

46. H.B. Yang, J.D. Rameau, Z.H. Pan, G.D. Gu, P.D. Johnson, H. Claus, D.G. Hinks, T.E. Kidd, Phys. Rev. Lett. **107**, 047003 (2011). DOI 10.1103/PhysRevLett.107.047003

47. Y. Kohsaka, C. Taylor, P. Wahl, A. Schmidt, J. Lee, K. Fujita, J.W. Alldredge, K. McElroy, J. Lee, H. Eisaki, S. Uchida, D.H. Lee, J.C. Davis, Nature (London) **454**, 1072 (2008). DOI 10.1038/nature07243

48. K.A.G. Fisher, E.J. Nicol, J.P. Carbotte, EPL (Europhysics Letters) **95**, 47008 (2011). DOI 10.1209/0295-5075/95/47008

49. E. Bascones, B. Valenzuela, Phys. Rev. B **77**, 024527 (2008). DOI 10.1103/PhysRevB.77.024527

50. A.J.H. Borne, J.P. Carbotte, E.J. Nicol, Phys. Rev. B **82**, 024521 (2010). DOI 10.1103/PhysRevB.82.024521

51. A. Pushp, C.V. Parker, A.N. Pasupathy, K.K. Gomes, S. Ono, J. Wen, Z. Xu, G. Gu, A. Yazdani, Science **324**, 1689 (2009). DOI 10.1126/science.1174338

52. J.W. Loram, J.L. Tallon, W.Y. Liang, Phys. Rev. B **69**, 060502 (2004). DOI 10.1103/PhysRevB.69.060502

53. J.P.F. LeBlanc, E.J. Nicol, J.P. Carbotte, Phys. Rev. B **80**, 060505(R) (2009). DOI 10.1103/PhysRevB.80.060505

54. A.J.H. Borne, J.P. Carbotte, E.J. Nicol, Phys. Rev. B **82**, 094523 (2010). DOI 10.1103/PhysRevB.82.094523

55. W.A. Huttema, J.S. Bobowski, P.J. Turner, R. Liang, W.N. Hardy, D.A. Bonn, D.M. Broun, Phys. Rev. B **80**, 104509 (2009). DOI 10.1103/PhysRevB.80.104509

56. J.P. Carbotte, K.A.G. Fisher, J.P.F. LeBlanc, E.J. Nicol, Phys. Rev. B **81**, 014522 (2010). DOI 10.1103/PhysRevB.81.014522

57. J.P. Carbotte, E. Schachinger, J. Phys.: Condens. Matter **25**, 165702 (2013). DOI 10.1088/0953-8984/25/16/165702

58. E. Illes, E.J. Nicol, J.P. Carbotte, Phys. Rev. B **79**, 100505 (2009). DOI 10.1103/PhysRevB.79.100505

59. A. Pound, J. Carbotte, E. Nicol, Eur. Phys. J. B **81**, 69 (2011). DOI 10.1140/epjb/e2011-20096-y

60. J. Hwang, T. Timusk, G.D. Gu, J. of Phys.: Condensed Matter **19**(12), 125208 (2007). DOI 10.1088/0953-8984/19/12/125208

61. P. Bhalla, N. Singh, Eur. Phys. J. B **87**, 213 (2014). DOI 10.1140/epjb/e2014-50363-2

62. T.S. DeNobrega, J.P. Carbotte, Phys. Rev. B **83**, 094504 (2011). DOI 10.1103/PhysRevB.83.094504

63. P.E.C. Ashby, J.P. Carbotte, Phys. Rev. B **87**, 184514 (2013). DOI 10.1103/PhysRevB.87.184514

64. C.C. Homes, T. Timusk, R. Liang, D.A. Bonn, W.N. Hardy, Phys. Rev. Lett. **71**, 1645 (1993). DOI 10.1103/PhysRevLett.71.1645

65. J.P. Carbotte, E. Schachinger, Phys. Rev. B **86**, 224512 (2012). DOI 10.1103/PhysRevB.86.224512

66. D.N. Basov, S.I. Woods, A.S. Katz, E.J. Singley, R.C. Dynes, M. Xu, D.G. Hinks, C.C. Homes, M. Strongin, Science **283**, 49 (1999). DOI 10.1126/science.283.5398.49

67. B. Valenzuela, E. Bascones, Phys. Rev. Lett. **98**, 227002 (2007). DOI 10.1103/PhysRevLett.98.227002

68. J.P.F. LeBlanc, J.P. Carbotte, E.J. Nicol, Phys. Rev. B **81**, 064504 (2010). DOI 10.1103/PhysRevB.81.064504

69. M. Le Tacon, A. Sacuto, A. Georges, G. Kotliar, Y. Gallais, D. Colson, A. Forget, Nature Phys. **2**, 537 (2006). DOI 10.1038/nphys362

70. W. Guyard, M. Le Tacon, M. Cazayous, A. Sacuto, A. Georges, D. Colson, A. Forget, Phys. Rev. B **77**, 024524 (2008). DOI 10.1103/PhysRevB.77.024524

71. S. Hüfner, M.A. Hossain, A. Damascelli, G.A. Sawatzky, Rep. Prog. Phys. **71**, 062501 (2008). DOI 10.1088/0034-4885/71/6/062501

72. K.Y. Yang, K. Huang, W.Q. Chen, T.M. Rice, F.C. Zhang, Phys. Rev. Lett. **105**, 167004 (2010). DOI 10.1103/PhysRevLett.105.167004

73. P.A. Lee, Phys. Rev. Lett. **71**, 1887 (1993). DOI 10.1103/PhysRevLett.71.1887

74. A.C. Durst, P.A. Lee, Phys. Rev. B **62**, 1270 (2000). DOI 10.1103/PhysRevB.62.1270

75. M. Sutherland, D.G. Hawthorn, R.W. Hill, F. Ronning, S. Wakimoto, H. Zhang, C. Proust, E. Boaknin, C. Lupien, L. Taillefer, R. Liang, D.A. Bonn, W.N. Hardy, R. Gagnon, N.E. Hussey, T. Kimura, M. Nohara, H. Takagi, Phys. Rev. B **67**, 174520 (2003). DOI 10.1103/PhysRevB.67.174520

76. J.P. Carbotte, Phys. Rev. B **83**, 100508 (2011). DOI 10.1103/PhysRevB.83.100508

77. A.J.A. James, R.M. Konik, T.M. Rice, Phys. Rev. B **86**, 100508(R) (2012). DOI 10.1103/PhysRevB.86.100508

78. A. Kanigel, U. Chatterjee, M. Randeria, M.R. Norman, S. Souma, M. Shi, Z.Z. Li, H. Raffy, J.C. Campuzano, Phys. Rev. Lett. **99**, 157001 (2007). DOI 10.1103/PhysRevLett.99.157001

79. E. Schachinger, J.P. Carbotte, Phys. Rev. B **81**, 214521 (2010). DOI 10.1103/PhysRevB.81.214521